Turing patterns and apparent competition in predator-prey food webs on networks

L. D. Fernandes and M. A. M. de Aguiar
Instituto de Física "Gleb Wataghin," Universidade Estadual de Campinas (UNICAMP) 13083-970, Campinas, Brazil
(Received 13 July 2012; published 5 November 2012)

Reaction-diffusion systems may lead to the formation of steady-state heterogeneous spatial patterns, known as Turing patterns. Their mathematical formulation is important for the study of pattern formation in general and plays central roles in many fields of biology, such as ecology and morphogenesis. Here we show that Turing patterns may have a decisive role in shaping the abundance distribution of predators and prey living in patchy landscapes. We extend the original model proposed by Nakao and Mikhailov [Nat. Phys. **6**, 544 (2010)] by considering food chains with several interacting pairs of prey and predators distributed on a scale-free network of patches. We identify patterns of species distribution displaying high degrees of apparent competition driven by Turing instabilities. Our results provide further indication that differences in abundance distribution among patches can be generated dynamically by self organized Turing patterns and not only by intrinsic environmental heterogeneity.

DOI: 10.1103/PhysRevE.86.056203 PACS number(s): 89.75.Kd, 87.23.Cc

I. INTRODUCTION

Reaction-diffusion systems in which two or more species interact locally and diffuse through the medium have long been focus of studies in many different fields, such as physics, chemistry, and biology. Part of the interest in these systems is related to their potential to form self-organized spatiotemporal patterns, like traveling and spiral waves [1] or stationary patterns, called Turing patterns [2].

Since Turing's classic work on morphogenesis [3], a large number of models and applications of reaction-diffusion systems in chemistry and biology have been studied. These include theoretical [4–9], experimental [10–14] and, more recently, empirical [15]. A key theoretical contribution was given by Mimura and Murray [6], who applied Turing's idea to understand patchiness in continuously distributed predator-prey populations.

Recently, Nakao and Mikhailov [16] proposed a discrete version of the prey-predator model of Mimura and Murray [6] in which the species are organized in patches, instead of being continuously distributed in space. The patches can be represented as nodes of a complex network such that predators and prey interact locally in each patch and diffuse through connected nodes. The patterns obtained in Ref. [16] display significant differences when compared to the patterns obtained in continuously distributed species.

In the present work we extend of the model of Nakao and Mikhailov [16] by considering food chains with more than two species. We study the dynamics of several pairs of prey and predators that interact by consuming common prey. We show that the Turing patterns of population density displayed by the system present nontrivial correlations in the abundance distributions. In particular, we observe the emergence of strong competition between prey of adjacent species in the food chain, despite the fact that no direct competition between them is included in the equations. These correlations are strictly related to diffusion and correspond to a new mechanism of *apparent competition*, driven by Turing instabilities instead of local interactions. We characterize these patterns using numerical simulations and mean-field approximations. We also discuss the relevance of these results to patterns of species distribution in real trophic systems.

II. DYNAMICAL MODEL

The reaction-diffusion system studied by Mimura and Murray [6] describes the interaction between one species of prey and one species of predator that interact locally and diffuse through a continuous physical environment. If the diffusion coefficient of the predators is sufficiently larger than that of the prey, the solution corresponding to the uniform distribution of individuals through space becomes unstable to spatial perturbations and patterns of density develop. As shown by Nakao and Mikhailov [16], this scenario persists when the medium is replaced by a network of patches, although the qualitative nature of the patterns change considerably.

Here we extend the model of Nakao and Mikhailov by considering larger food chains, composed of several species of prey and predators. We assume that each prey species has a primary predator associated to it, forming a pair. The pairs in the food chain are hierarchically coupled by secondary predation relations. Thus, the prey in the first pair is consumed by its main predator and also by the predator in the second pair, though with the lower intensity γ. Similarly, the prey of the second pair is consumed primarily by its associated predator and also by the predator of the third pair, and so on. Only the last species of prey in this ordered chain is consumed exclusively by its main predator, as illustrated in Fig. 1. Although the resulting food chain is greatly simplified, predators in the top layers can represent larger predators, which are known to feed from a wider range of body size prey than smaller ones [17]. Links connecting prey to tertiary predators up the chain could also be added but do not result in qualitatively different patterns. These links, therefore, were not included.

The environment where these interactions take place consists of a network of patches. Species-species interactions, as described by the food chain, take place locally in each patch and the coupling between patches occurs exclusively via diffusion, which is possible if the patches are connected in the network.

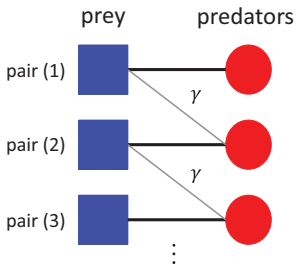

FIG. 1. (Color online) Hierarchical food chain with three pairs of prey and predators. Each predator is linked to the previous prey (secondary predation) with strength γ.

The equations describing this dynamical system are given by

$$\begin{aligned}\frac{d}{dt}u_i^{(l)}(t) &= f\left(u_i^{(l)},v_i^{(l)}\right) - \gamma u_i^{(l)}v_i^{(l+1)} + \varepsilon\sum_j L_{ij}u_j^{(l)},\\ \frac{d}{dt}v_i^{(l)}(t) &= g\left(u_i^{(l)},v_i^{(l)}\right) + \phi\gamma u_i^{(l-1)}v_i^{(l)} + \sigma\varepsilon\sum_j L_{ij}v_j^{(l)},\end{aligned} \tag{1}$$

where $u_i^{(l)}(t)$ and $v_i^{(l)}(t)$ represent the populations of prey and predators at time t, respectively. The label $l = 1,2,3,\ldots,$ index the prey-predator pair.

The functions f and g describe the local interaction between prey and predators of each pair (also called *reaction functions*). The terms proportional to γ represent the secondary predation relations between adjacent pairs and the parameter ϕ accounts for the ratio between predator gain and prey loss in the secondary interaction.

The parameters ε and σ are, respectively, the prey mobility and the ratio between predator and prey mobilities. The matrix L stands for the *Laplacian matrix* and accounts for the diffusion of populations across connected sites. For undirected networks, L is symmetric with $L_{ij} = A_{ij} - k_i\delta_{ij}$, where A is the *adjacency matrix* and k_i the degree of node i. The adjacency matrix defines the topology of the network and is given by $A_{ij} = 1$ if nodes i and j are connected and $A_{ij} = 0$ if they are not. The degree $k_i = \sum_j A_{ij}$ is the number of connections of node i.

The term $\sum_j L_{ij}u_j^{(l)}$ in Eq. (1) controls the diffusion of prey $u^{(l)}$. It gives the difference between the total population of prey $u^{(l)}$ in the sites connected to i and k_i times the population in the site i. If $u^{(l)}$ is the same in all sites the sum adds to zero and there is no diffusion. A similar term controls the diffusion of predators in the equation for $v^{(l)}$.

As a simplification, we consider that the intrinsic growth rate of all prey species are the same, as is the intrinsic death rate of all predator species. In that manner, the functions f and g and the parameters associated to these functions are the same for all pairs. The more general case in which the parameters for each pair differ is discussed in Sec. VII.

The functions f and g are chosen according to the model of Mimura and Murray [6],

$$\begin{aligned}f(u,v) &= \left(\frac{a+bu-u^2}{c} - v\right)u,\\ g(u,v) &= [u-(1+dv)]v,\end{aligned} \tag{2}$$

where a, b, c, and d are positive parameters that will be fixed to $a = 35$, $b = 16$, $c = 9$, and $d = 0.4$ throughout this paper [6].

Both the prey-per-capita growth rate and the pradator-per-capita death rate are density dependent. The hump effect that can be noted in the prey growth in f represents what in biology is called the *Allee effect* [23–25], describing a positive correlation between population density and per capita growth rate in small populations. The linear function related to the predator per capita death rate accounts for intraspecific competition in the predator population.

The possibility of observing Turing patterns for these equations must be evaluated via linear analysis. Here we show the analysis for the case of a single prey-predator pair and of two prey-predator pairs. The general case with n pairs is slightly more complicated but can be done following the same lines.

III. LINEAR STABILITY ANALYSIS

In this section we briefly review the stability analysis of network organized systems. For simplicity we consider only up to two pairs of prey and predator, since the methodology generalizes immediately to the case of higher numbers of pairs.

For the case of only one pair, the equilibrium populations in the absence of diffusion, $(\bar{u},\bar{v})$, are the positive solution of

$$f(\bar{u},\bar{v}) = 0, \quad g(\bar{u},\bar{v}) = 0. \tag{3}$$

Diffusion-driven instability occurs when the equilibrium is stable against perturbations in the absence of diffusion ($\varepsilon = 0.0$) but is unstable when diffusion is considered.

Let

$$(u_i,v_i) = (\bar{u},\bar{v}) + (\delta u_i,\delta v_i) \tag{4}$$

be small perturbations to the fixed point $(\bar{u},\bar{v})$ at site i. Substituting (4) in Eq. (1) and linearizing, we obtain

$$\begin{aligned}\frac{d}{dt}\delta u_i &= f_u\delta u_i + f_v\delta v_i + \varepsilon\sum_{j=1}^{N} L_{ij}\delta u_i,\\ \frac{d}{dt}\delta v_i &= g_u\delta u_i + g_v\delta v_i + \sigma\varepsilon\sum_{j=1}^{N} L_{ij}\delta v_i,\end{aligned} \tag{5}$$

where the derivatives are evaluated at the equilibrium.

Since we are dealing with network-organized systems, it is convenient to expand the perturbations in the basis formed by the eigenvectors of the Laplacian matrix, $\{\vec{\Phi}^{\alpha}\}$ [16]. Here $\alpha = 1,\ldots,N$ represent different modes, in direct analogy with the Fourier modes that appear in continuous systems where the

TABLE I. Homogeneous fixed points for different values of γ for the four-species system.

γ	$u^{(1)}$	$v^{(1)}$	$u^{(2)}$	$v^{(2)}$
0.002	4.989	9.973	4.993	9.995
0.01	4.945	9.863	4.966	9.977
0.05	4.726	9.314	4.837	9.889

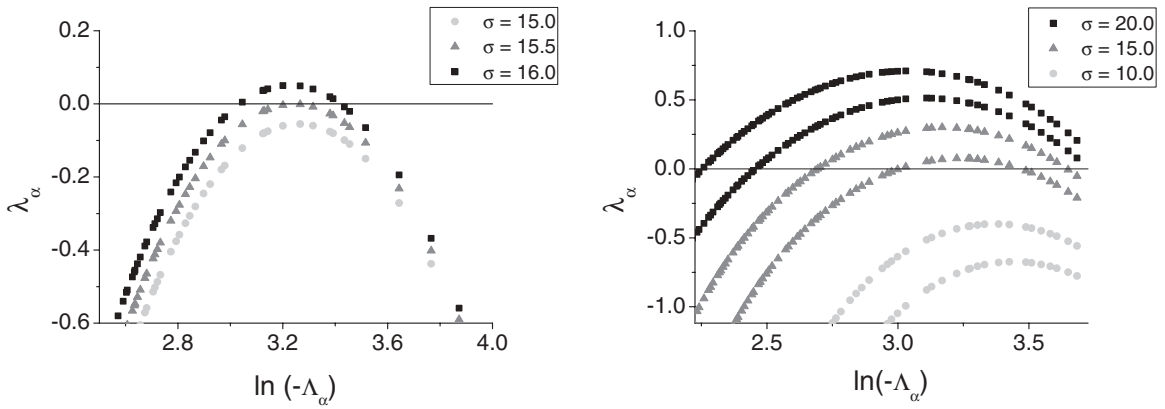

FIG. 2. Linear growth rates, λ_α, as a function of the eigenvalues of the Laplacian, Λ_α, for a Barabási-Albert network with $N = 200$ and $\langle k \rangle = 10$, for (a) one prey-predator pair and (b) two pairs. In all the cases $\varepsilon = 0.06$ and three different values of σ are shown for comparison. Modes with $\lambda_\alpha > 0.0$ are observed for σ above the critical value in each case.

Laplacian is the usual operator ∇^2. We find

$$\delta u_i(t) = \sum_{\alpha=1}^{N} c_\alpha \exp[\lambda_\alpha t]\phi_i^{(\alpha)}, \qquad \delta v_i(t) = \sum_{\alpha=1}^{N} c_\alpha B_\alpha \exp[\lambda_\alpha t]\phi_i^{(\alpha)}. \tag{6}$$

Substituting (6) in Eq. (5) and using $\sum_{j=1}^{N} L_{ij}\phi_j^{(\alpha)} = \Lambda_\alpha \phi_i^{(\alpha)}$, we obtain, for each mode α,

$$\lambda_\alpha \begin{pmatrix} 1 \\ B_\alpha \end{pmatrix} = \begin{pmatrix} f_u + \varepsilon\Lambda_\alpha & f_v \\ g_u & g_v + \sigma\varepsilon\Lambda_\alpha \end{pmatrix} \begin{pmatrix} 1 \\ B_\alpha \end{pmatrix}. \tag{7}$$

The matrix obtained in Eq. (7) is the Jacobian of the system with diffusion. The linear growth rates, λ_α, of each mode are, as expected, the eigenvalues of the Jacobian matrix. Turing instability appears when one of the modes becomes unstable. At the threshold, $\mathrm{Re}(\lambda_\alpha) = 0$ for some $\alpha = \alpha_c$ and $\mathrm{Re}(\lambda_\alpha) < 0$ for all other modes.

Above this threshold $\mathrm{Re}(\lambda_{\alpha_c}) > 0$ and perturbations grow in time according to $\exp[\lambda_\alpha t]$, eventually forming the stationary Turing pattern. A necessary condition for this is that the solutions of (5) are confined, otherwise the perturbed solution diverges.

The same procedure can be used to analyze systems with more than one pair. After linearizing the equations around the equilibrium state [given by the fixed point of system (1) in the absence of diffusion; see Table I] and expanding the perturbations in the eigenvectors of the Laplacian matrix, we obtain the Jacobian matrix. For two pairs, we obtain

$$\begin{pmatrix} f_u + \varepsilon\Lambda_\alpha & f_v & 0 & -\gamma u \\ g_u & g_v + \sigma\varepsilon\Lambda_\alpha & 0 & 0 \\ 0 & 0 & f_u + \varepsilon\Lambda_\alpha & f_v \\ \phi\gamma u & 0 & g_u & g_v + \sigma\varepsilon\Lambda_\alpha \end{pmatrix}. \tag{8}$$

In the case of two or more pairs of species it is not possible to obtain the eigenvalues of the Jacobian analytically (see Appendix A for calculation with one pair), which must be computed numerically. For each value of Λ_α there will be at most four real eigenvalues of the Jacobian, but only two of

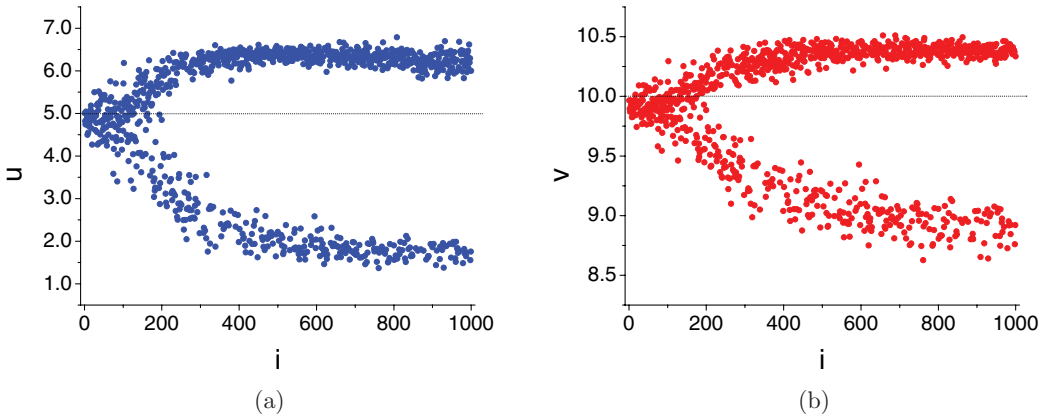

FIG. 3. (Color online) Stationary abundance patterns for a single predator-prey pair as a function of node index i for $\varepsilon = 0.12$ and $\sigma = 20.0$ for (a) prey and (b) predators. The lines at $u_i = 5.0$ and $v_i = 10.0$ indicate the values of the homogeneous state, which is a fixed point for this set of parameters.

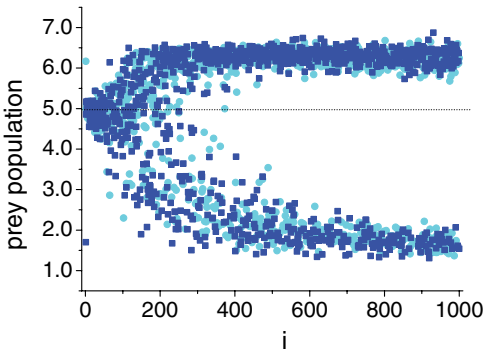

FIG. 4. (Color online) Stationary abundance patterns for $u^{(1)}$ (circles) and $u^{(2)}$ (squares) as a function of node index i for $\varepsilon = 0.12$, $\sigma = 20.0$, $\phi = 0.5$, and $\gamma = 0.002$.

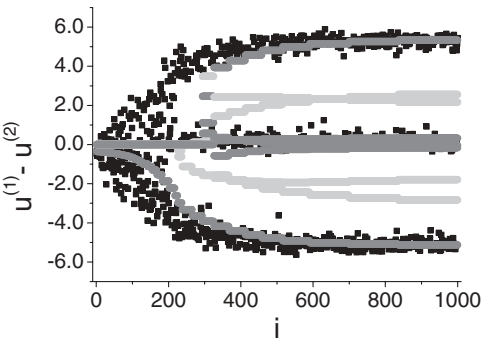

FIG. 6. Stationary pattern for the difference $u^{(1)} - u^{(2)}$ as obtained from simulations (black) and from the mean-field approximation (gray and light gray) for $\varepsilon = 0.12$, $\sigma = 20.0$, $\phi = 0.5$, and $\gamma = 0.05$. The light gray values represent unstable branches.

them may become positive. This is similar to the case of one pair of species, which has at most two real eigenvalues for each Λ_α, but only one can become positive.

Figure 2 shows the linear growth rates, λ_α, as a function of the eigenvalues of the Jacobian, Λ_α for $a = 35.0$, $b = 16.0$, $c = 9.0$, $d = 0.4$, and $\varepsilon = 0.06$, and a network of $N = 200$ nodes with power-law degree distribution constructed according to the Barabási-Albert algorithm [18]. Figure 2(a) shows the growth rates for the system with one pair and 2(b) for the system with two pairs.

IV. TWO SPECIES

We first review the case of two species as a reference to the more complex patterns we study in the following sections. We consider a network with $N = 1000$ nodes, constructed according to the Barabási-Albert model [18]. The populations of prey, u_i, and predators, v_i, defined in each node i interact locally and diffuse through the network nodes according to Eqs. (1), with $l = 1$ (and $u_i^{(0)} = v_i^{(2)} = 0$). Equations (1) are numerically integrated until a stationary distribution of the species abundance is obtained.

Figure 3 shows the stationary abundance patterns of prey, Fig. 3(a), and predators, Fig. 3(b), as a function of node index i for $\varepsilon = 0.12$ and $\sigma = 20.0$. The nodes are ordered according to decreasing degree k_i.

The pattern of prey distribution is formed by two groups of nodes presenting significant differentiation in relation to the homogeneous state: a group with high abundance (values of u_i well above $\bar{u}$) and a group with low abundance (values of u_i well below $\bar{u}$). The pattern of predators follows directly the pattern of the prey: nodes with large abundance of prey ($u_i > \bar{u}$) also have large abundance of predators ($v_i > \bar{v}$) and vice versa.

V. FOUR SPECIES

The four-species system is described by Eq. (1) with $l = 1,2$ (and $u_i^{(0)} = v_i^{(3)} = 0$). The equations have a homogeneous equilibrium point that depends on the coupling parameter γ, as displayed by Table I. The populations of prey and predators decrease as γ increases.

The stationary patterns of prey $u^{(1)}$ and $u^{(2)}$ as a function of the node index i are shown in Fig. 4. These patterns of abundance (and also those of $v^{(1)}$ and $v^{(2)}$) do not differ very much from each other or from the previous case shown in Fig. 3. In particular, both types of prey and predators present the separation of nodes in high-abundance and low-abundance groups.

However, this similarity is partly an illusion, having to do with the way the data are plotted. Indeed, a new underlying pattern arises when the difference between the prey abundances $u_i^{(1)} - u_i^{(2)}$ is plotted, as shown in Fig. 5 for different values of the coupling strength γ.

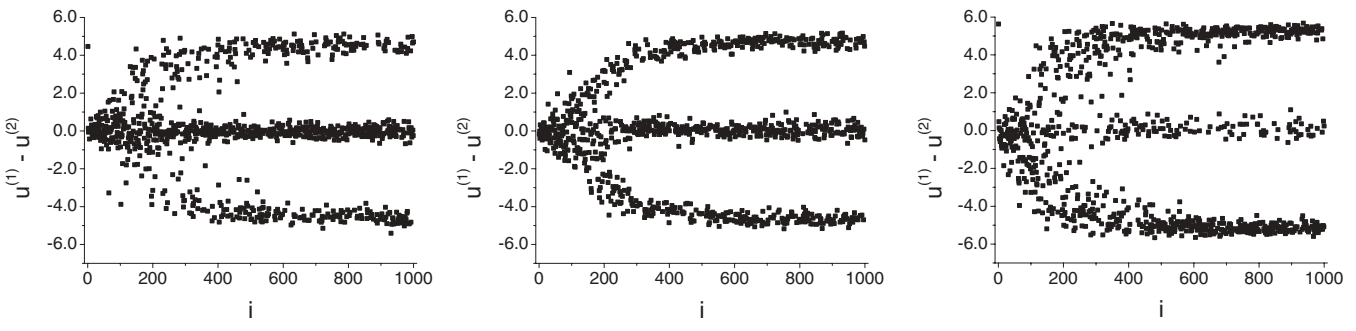

FIG. 5. Stationary patterns for the difference $u^{(1)} - u^{(2)}$ as a function of node index i for (a) $\gamma = 0.002$, (b) $\gamma = 0.01$, and (c) $\gamma = 0.05$. In all cases $\varepsilon = 0.12$, $\sigma = 20.0$, and $\phi = 0.5$.

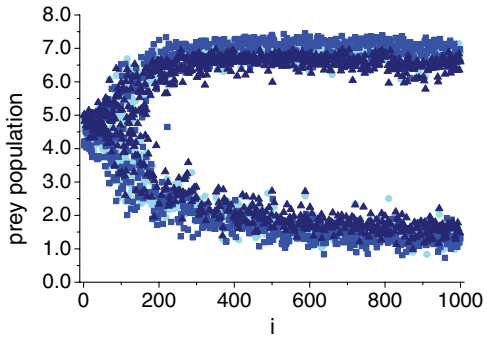

FIG. 7. (Color online) Stationary patterns of prey distributions as a function of node index i for the case of three pairs for $\varepsilon = 0.12$, $\sigma = 20.0$, $\phi = 0.5$, and $\gamma = 0.05$. Here, $u^{(1)}$ are circles, $u^{(2)}$ squares, and $u^{(3)}$ triangles.

In all cases, it is possible to distinguish three main branches: the upper branch, where $u^{(1)} - u^{(2)} \approx 4$, corresponding to nodes where $u^{(1)}$ is abundant but $u^{(2)}$ is not; the lower branch, where $u^{(1)} - u^{(2)} \approx -4$ where the abundances are reversed; and the middle branch, where $u^{(1)} - u^{(2)} \approx 0$ and $u^{(1)}$ and $u^{(2)}$ have similar abundances. This configuration of branches can be derived via a mean-field approximation [26,27], as discussed in Appendix B and displayed in Fig. 6.

As γ increases the middle branch gets less populated and the nodes are dominated mostly by a single species of prey and predator. This corresponds to a strong effect of apparent competition driven by Turing instabilities. The more important the secondary predation (which is kept weaker than the direct predation in the each pair), the stronger the effect.

VI. SIX SPECIES

To investigate if the negative correlation between prey of coupled pairs also occur in larger trophic chains we consider a system with six species, again given by Eq. (1) with $l = 1,2,3$ (and $u_i^{(0)} = v_i^{(4)} = 0$). The stationary patterns of prey distributions are shown in Fig. 7.

Once again, for each prey species, the nodes cluster into groups of high and low abundances. The analysis of the correlations between different prey species, however, is now more involved. We first define the quantity

$$\sigma_i^{(l)} = \mathrm{sng}\left(u_i^{(l)} - \bar{u}^{(l)}\right) = \begin{cases} +1, & \text{if} \quad u_i^{(l)} > \bar{u}^{(l)} \\ -1, & \text{if} \quad u_i^{(l)} < \bar{u}^{(l)} \end{cases}, \tag{9}$$

where $\sigma_i^{(l)}$ indicates if the l-th prey population at node i has high ($\sigma_i^{(l)} = +1$) or low ($\sigma_i^{(l)} = -1$) abundance with respect to the homogeneous value.

Second, we separate the nodes in two groups: those with $\sigma^{(2)} = +1$ and those with $\sigma^{(2)} = -1$. Since nodes with large k_i are not sensitive to the coupling, we restrict this analysis to nodes with $i \geqslant 250$, for which the differentiation is more evident. Finally, we focus on the value of the sum $\sigma^{(1)} + \sigma^{(3)}$ for these nodes. The three possible values of this sum indicate the following situations: If $\sigma^{(1)} + \sigma^{(3)} = +2$, both $u^{(1)}$ and $u^{(3)}$

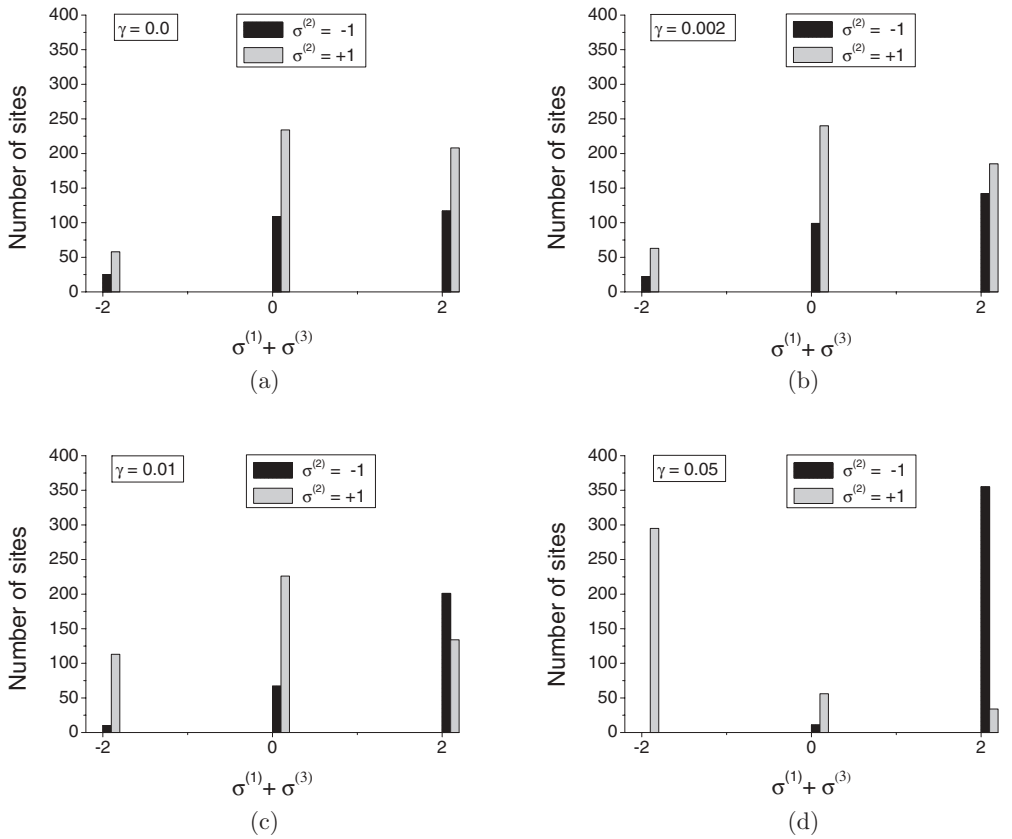

FIG. 8. Histogram of nodes with different values of $\sigma^{(1)} + \sigma^{(3)}$ for $\sigma^{(2)} = -1$ (black bars) and $\sigma^{(2)} = +1$ (gray bars) for (a) $\gamma = 0.0$, (b) $\gamma = 0.002$, (c) $\gamma = 0.01$, and (d) $\gamma = 0.05$.

have high abundance in the node; if $\sigma^{(1)} + \sigma^{(3)} = -2$, both $u^{(1)}$ and $u^{(3)}$ have low abundance and if $\sigma^{(1)} + \sigma^{(3)} = 0$, $u^{(1)}$ and $u^{(3)}$ have opposed abundance characteristics. If the hypothesis of negative correlation is to be valid, the group of nodes with $\sigma^{(2)} = +1$ must have most of its node with $\sigma^{(1)} + \sigma^{(3)} = -2$ and the group with $\sigma^{(2)} = -1$ must have most of its nodes with $\sigma^{(1)} + \sigma^{(3)} = +2$. The results are shown in Fig. 8 in the form of histograms.

In Fig. 8(a) $\gamma = 0.0$ and the three prey distributions are uncorrelated. Figures 8(b) and 8(c) display cases with increasing values of γ. As the coupling strength increases, the number of nodes with $\sigma^{(1)} + \sigma^{(3)} = +2$ increases in the group with $\sigma^{(2)} = -1$ and similarly with the number of nodes with $\sigma^{(1)} + \sigma^{(3)} = -2$ in the group where $\sigma^{(2)} = +1$. This separation is evident in Fig. 8(d), where $\gamma = 0.05$, where it is clear that most of the nodes where $u^{(2)}$ has large abundance display low abundances of both $u^{(1)}$ and $u^{(3)}$ and vice versa, showing the persistence of the negative correlation between prey of coupled pairs.

VII. DISCUSSION

We have studied the formation of Turing patterns in an extended prey-predator system, considering trophic chains composed of one, two, and three prey-predator pairs, coupled by cross predation and dispersing through the connected nodes of a complex network. We detected the emergence of negative correlations between the populations of prey of coupled pairs in each node, even though there are no direct competition between prey in the equations. This effect, known in biology as apparent competition [28,29], is triggered here by the Turing instabilities and not by the local interactions.

The description of fragmented landscapes as complex networks is relatively recent in ecology [19]. Although large landscape networks have been studied [30], most of the empirical work has dealt with a relatively small number of patches [31] and it is not obvious that the patterns observed here for networks with $N = 1000$ nodes persist in smaller sets. We have checked that for N as low as 100 the same pattern of apparent competition can be clearly identified but not so much for $N = 50$, which seems to be a limiting size for the present set of parameters.

Another important concern in the application of our results to realist ecological problems is the topology of the network. All numerical simulations presented in the previous sections were performed for networks exhibiting power-law decay of the degree distribution that results from the application of the Barabási-Albert algorithm. Natural landscape networks can exhibit significant heterogeneity in the degree distribution [20] but are not necessarily scale free. In order to verify the robustness of our results against changes in the network topology, we have also simulated networks with Poisson degree distribution, associated to random networks. We found that the negative correlations between prey still holds for $N = 1000$ and average degree $\langle k \rangle = 20$.

The dynamical equations considered in this paper were greatly simplified by the use of the same set of parameters for each pair of predator-prey species. This, however, results in a ecological model in which all prey and predators have the same intrinsic birth and death rates, which is unrealistic in real-world hierarchically organized food chains. In order to investigate less symmetric equations we have fixed $c = 9$ and $d = 0.4$ for all the pairs but set $c^{(l)} = (1.1)^{l-1}c$ and $d^{(l)} = (1.1)^{l-1}d$, where l is the index of each pair. In this manner, the prey of each pair have birth rates that are 10% smaller than the prey of the preceding pair. Similarly, the predators of a pair have death rates 10% larger than the preceding predators on the chain. The results for this new set of parameters, considering a Barabási-Albert network with $N = 1000$ and $\langle k \rangle = 20$, displayed Turing patterns for the abundance distributions of prey and predators that were very similar to those presented in the previous sections, including the strong apparent competition observed between prey of adjacent pairs.

We have also varied the diffusion rates for the case of two pairs of species. Using the same set of parameters for the functions f and g and the same network topology as in Sec. V, we first fixed $\sigma = 20.0$ for both pairs and set $\varepsilon_1 = 0.12$ and $\varepsilon_2 = 0.06$. The resulting Turing patterns differed slightly from the case where $\varepsilon_1 = \varepsilon_2 = 0.12$ but also displayed the negative correlation observed in that case. Next we fixed $\varepsilon = 0.12$ for both pairs and (i) $\sigma_1 = 15.0$ and $\sigma_2 = 20.0$ and (ii) $\sigma_1 = 20.0$ and $\sigma_2 = 15.0$. In both cases, Turing patterns formed, even though $\sigma = 15.0$ is below the critical value for pattern formation for a single isolated pair. The negative correlation between the species of each pair was also observed for strong coupling, confirming the robustness of apparent competition driven by Turing instabilities in the system.

The occurrence of Turing patterns in real ecological systems is still an open question. This is in part due to the difficulties in conducting controlled ecological field experiments to distinguish between patterns related to space heterogeneity or to intrinsic mechanisms of the interaction. However, there is growing evidence of species distribution patterns formed by the Turing mechanism [21,22].

Our results point to the possibility that, at least in part, species abundance patterns might be related to Turing instabilities and not to environmental heterogeneity. Moreover, strong effects of apparent competition might emerge spontaneously driven by Turing instabilities and not necessarily by local interactions.

ACKNOWLEDGMENTS

It is a pleasure to thank Carolina Reigada for important discussions. This work was partly supported by FAPESP and CNPq.

APPENDIX A: CRITICAL VALUE FOR TURING INSTABILITY

The eigenvalues of the Jacobian matrix of Eq. (7) are given by the roots of the characteristic polynomial

$$\lambda_\alpha^2 - \lambda_\alpha(f_u + g_v + (1+\sigma)\varepsilon\Lambda_\alpha) + (f_u + \varepsilon\Lambda_\alpha)(g_v + \sigma\varepsilon\Lambda_\alpha) - f_v g_u = 0,$$

which are given by

$$\lambda_\alpha = \frac{f_u + g_v + (1+\sigma)\varepsilon\Lambda_\alpha \pm \sqrt{4 f_v g_u + (f_u - g_v + (1-\sigma)\varepsilon\Lambda_\alpha)^2}}{2}. \tag{A1}$$

For each mode α there are two possible values for λ_α, but only the one associated to the plus sign can become positive, so we only need to consider this eigenvalue. Solving $d(\lambda_\alpha)/d(\Lambda_\alpha) = 0$ we obtain the critical Laplacian eigenvalue. Substituting this value in Eq. (A1) and imposing that $\mathrm{Re}(\lambda_{\alpha_c}) = 0$ in the instability threshold, we obtain the critical value σ_c,

$$\sigma_c = \frac{f_u g_v - 2 f_v g_u + 2\sqrt{f_v g_u (f_v g_u - f_u g_v)}}{f_u^2}. \tag{A2}$$

APPENDIX B: MEAN-FIELD APPROXIMATION

The mean-field approximation consists in averaging the heterogeneous degree distribution of the network by adjusting the strength by which each node senses the presence of its neighbors. Introducing the local fields

$$\begin{aligned} x_i^l &= \sum_{j=1}^{N} A_{ij} u_j^{(l)} \\ y_i^l &= \sum_{j=1}^{N} A_{ij} v_j^{(l)} \end{aligned} \tag{B1}$$

and substituting in Eq. (1), we obtain

$$\begin{aligned} \frac{d}{dt} u_i^{(l)}(t) &= f\left(u_i^{(l)}, v_i^{(l)}\right) - \gamma u_i^{(l)} v_i^{(l+1)} + \varepsilon\left(x_i^l - k_i u_i^{(l)}\right), \\ \frac{d}{dt} v_i^{(l)}(t) &= g\left(u_i^{(l)}, v_i^{(l)}\right) + \phi\gamma u_i^{(l-1)} v_i^{(l)} + \sigma\varepsilon\left(y_i^l - k_i v_i^{(l)}\right). \end{aligned} \tag{B2}$$

We then consider the approximations $x_i^l \simeq k_i X^l$ and $y_i^l \simeq k_i Y^l$, where the global fields X and Y are defined as the weighted averages

$$X^l = \sum_{j=1}^{N} w_j u_i^{(l)}, \quad Y^l = \sum_{j=1}^{N} w_j v_i^{(l)}, \tag{B3}$$

with the weights

$$w_j = k_j \Big/ \sum_{l=1}^{N} k_l. \tag{B4}$$

This choice gives hubs have a stronger influence in the calculation of the global fields.

With this approximation, and introducing the parameter $\beta(i) = \varepsilon k_i$, the dynamical system may be written as

$$\begin{aligned} \frac{d}{dt} u^{(l)}(t) &= f(u^{(l)}, v^{(l)}) - \gamma u^{(l)} v^{(l+1)} + \beta(X^l - u^{(l)}), \\ \frac{d}{dt} v^{(l)}(t) &= g(u^{(l)}, v^{(l)}) + \phi\gamma u^{(l-1)} v^{(l)} + \sigma\beta(Y^l - v^{(l)}), \end{aligned} \tag{B5}$$

where each dynamical variable interacts only with its associated global field. Since every node now possesses the same dynamical equation, we may drop the index i.

In order to describe the patterns for the difference of prey populations, in the case with two prey-predator pairs, we define the new variables,

$$u_\pm = u^{(1)} \pm u^{(2)}, \quad v_\pm = v^{(1)} \pm v^{(2)}. \tag{B6}$$

The system of Eqs. (B5), written with the new variables (B6), is given by

$$\begin{aligned} \frac{du_\pm}{dt} &= F_\pm(u_-, u_+, v_-, v_+) - \frac{\gamma}{4}(u_- + u_+)(v_+ - v_-) \\ &\quad + \beta(X^\pm - u_+), \\ \frac{dv_\pm}{dt} &= G_\pm(u_-, u_+, v_-, v_+) \pm \frac{\phi\gamma}{4}(u_- + u_+)(v_+ - v_-) \\ &\quad + \sigma\beta(Y^\pm - v_+), \end{aligned} \tag{B7}$$

where

$$\begin{aligned} F_\pm &= f(u^{(1)}(u_-, u_+), v^{(1)}(v_-, v_+)) \\ &\quad \pm f(u^{(2)}(u_-, u_+), v^{(2)}(v_-, v_+)), \\ G_\pm &= g(u^{(1)}(u_-, u_+), v^{(1)}(v_-, v_+)) \\ &\quad \pm g(u^{(2)}(u_-, u_+), v^{(2)}(v_-, v_+)), \end{aligned} \tag{B8}$$

and

$$X^\pm = X^1 \pm X^2, \quad Y^\pm = Y^1 \pm Y^2. \tag{B9}$$

If the global fields for each dynamical variable are given, the parameter β may be seen as a bifurcation parameter. It is possible to note a saddle-node bifurcation in the system and the appearance of new stable fixed points, when the value of β is increased from $\beta = 0$.

We obtain the global fields (B9) by numerically integrating equations (1) and using the stationary values of the dynamical variables in Eq. (B3) and these in Eq. (B9). We then construct bifurcation diagrams calculating, for each value of β, the fixed points of the system (B7). Since each node has an associated degree k_i and, therefore, an associated β, it is possible to project the bifurcation diagram in the stationary pattern that resulted of the numerical integration of Eq. (1). The projection of the bifurcation diagram relative to the variable u_- on the stationary pattern for the difference $u^{(1)} - u^{(2)}$ is shown in Fig. 6.

[1] J. Murray, *Mathematical Biology I: An Introduction* (Springer, New York, 2002).
[2] J. Murray, *Mathematical Biology II: Spatial Models and Biomedical Applications* (Springer, New York, 2003).
[3] A. M. Turing, Philos. Trans. R. Soc. London B **237**, 37 (1952).
[4] J. Murray, J. Theor. Biol. **98**, 143 (1982).
[5] J. Murray, Sci. Am. **258**, 80 (1988).
[6] M. Mimura and J. Murray, J. Theor. Biol. **75**, 249 (1978).
[7] A. Koch and H. Meinhardt, Rev. Mod. Phys. **66**, 1481 (1994).
[8] K. Kishimoto, J. Math. Biol. **16**, 103 (1982).
[9] M. Baurmann, T. Gross, and U. Feudel, J. Theor. Biol. **245**, 220 (2007).
[10] V. Castets, E. Dulos, J. Boissonade, and P. De Kepper, Phys. Rev. Lett. **64**, 2953 (1990).
[11] Q. Ouyang and H. L. Swinney, Nature **352**, 610 (1991).
[12] V. K. Vanag and I. R. Epstein, Phys. Rev. Lett. **87**, 228301 (2001).
[13] T. Bánsági, Jr., V. K. Vanag and I. R. Epstein, Science **331**, 1309 (2011).
[14] S. Sawai, Y. Maeda, and Y. Sawada, Phys. Rev. Lett. **85**, 2212 (2000).
[15] M. Yamaguchi, E. Yoshimoto, and S. Kondo, Proc. Natl. Acad. Sci. USA **104**, 4790 (2007).
[16] H. Nakao and A. S. Mikhailov, Nat. Phys. **6**, 544 (2010).
[17] J. E. Cohen, S. L. Pimm, P. Yodziz and J. Saldana, J. Animal Ecol. **62**, 67 (1993).
[18] R. Albert and A.-L. Barabási, Rev. Mod. Phys. **74**(1), 47 (2002).
[19] M. Hagen, W. D. Kissling, C. Rasmussen, M. A. M. de Aguiar, L. E. Brown, D. W. Carstensen *et al.*, Adv. Ecol. Res. **46**, 89 (2012).
[20] M. A. Fortuna, C. Gómez-Rodríguez, and J. Bascompte, Proc. R. Soc. London B **273**, 1429 (2006).
[21] M. Rietker and J. van de Koppel, Trends Ecol. Evol. **23**, 169 (2008).
[22] J. Maron and S. Harrison, Science **278**, 1619 (1997).
[23] F. Courchamp, T. Clutton-Brock, and B. Grenfell, Trends Ecol. Evol. **14**, 405 (1999).
[24] P. Stephens and W. Sutherland, Trends Ecol. Evol. **14**, 401 (1999).
[25] M. Begon, C. Townsend, and J. Harper, *Ecology: From Individuals to Ecosystems* (Wiley-Blackwell, Oxford, 2006).
[26] T. Ichinomiya, Phys. Rev. E **70**, 026116 (2004).
[27] H. Nakao and A. S. Mikhailov, Phys. Rev. E **79**, 036214 (2009).
[28] R. Holt and R. Lawton, Ann. Rev. Ecol. Systemat. **25**, 495 (1994).
[29] E. Chaneton and M. Bonsall, Oikos **88**, 380 (2000).
[30] E. S. Minor and D. L. Urban, Conserv. Biol. **22**, 297 (2008).
[31] D. Urban and T. Keitt, Ecology **82**, 1205 (2001).